









Cite this: *Environ. Sci.: Nano*, 2020, 7, 1942

# Polystyrene nano- and microplastic accumulation at Arabidopsis and wheat root cap cells, but no evidence for uptake into roots†

Stephen E. Taylor, <sup>ab</sup> Carolyn I. Pearce, <sup>b</sup> Karen A. Sanguinet,<sup>a</sup> Dehong Hu, <sup>c</sup> William B. Chrisler, <sup>c</sup> Young-Mo Kim, <sup>d</sup> Zhan Wang<sup>e</sup> and Markus Flury <sup>\*af</sup>

Association of plastic particles with plant roots could represent a pathway for human consumption of plastic and plastic-associated organic contaminants. Here, we investigated the uptake of spherical, negatively-charged, polystyrene nano- and microparticles by plant roots. We used negatively-charged, 40 nm and 1  $\mu\text{m}$  fluorescently-labeled polystyrene spheres and two plant species: Arabidopsis (*Arabidopsis thaliana*) and wheat (*Triticum aestivum*). Plants were grown from seeds to 5 days for wheat and 12 days for Arabidopsis, in agar growth media containing plastic spheres ( $0.029 \text{ g L}^{-1}$ ), and plant uptake of spheres was investigated by laser scanning confocal microscopy and pyrolysis gas chromatography-mass spectrometry (GC-MS). The confocal images of both plant species showed no evidence for active uptake of nano- and microsized polystyrene spheres during plant growth up to the 1 to 2 leaf growth stage. Pyrolysis GC-MS was unsuccessful because of the occurrence of natural styrene monomers in plant roots and insufficient detection limits. Both 40 nm and 1  $\mu\text{m}$  polystyrene spheres accumulated at the root surface of each species, particularly at the root tip, and were still found attached to the root surface after washing. However, there was no evidence of plastic particles in the internal root structure. Our results demonstrate the association and accumulation of plastics at root surface and cap cells.

Received 24th March 2020,  
Accepted 20th May 2020

DOI: 10.1039/d0en00309c

rsc.li/es-nano

## Environmental significance

Micro- and nanoplastics are emerging contaminants in terrestrial ecosystems. While it is unknown how much micro- and nanoplastics is present in soils, there is concern that plastic particles can impair soil organisms, including plants. Plants have been shown to take up metal nanoparticles, but no data are available on whether plastic nanoparticles can be taken up by plants. Here, we show that micro- and nanoplastics associate with plant roots through attachment to root cap cells, but we did not find evidence of uptake of plastic nanoparticles into the interior of the root. As such, root crops grown in plastic contaminated soil can be a vector for human exposure of plastics.

## 1 Introduction

Estimates for plastic loads to terrestrial systems far exceed those already found in aquatic systems.<sup>1,2</sup> It is estimated that

up to 430 000 tons of plastic per year is deposited through land-applied biosolids in European farmlands and up to 300 000 tons per year in North America.<sup>2</sup> The effects of micro- and nanosized plastic particles in terrestrial systems are an emerging concern because of their observed prevalence,<sup>3</sup> atmospheric deposition to remote mountain ecosystems,<sup>4</sup> negative effects on living organisms,<sup>3,5</sup> and role in transporting metal<sup>6</sup> and organic<sup>7,8</sup> contaminants. Both metal<sup>6,9</sup> and persistent organic compounds including polychlorinated biphenyls (PCBs), polycyclic aromatic hydrocarbons (PAHs), hexachlorocyclohexanes (HCHs), along with other classes of polar and non-polar contaminants<sup>7,8,10</sup> have been shown to bind with nano- and microplastic particles, leading to increased contaminant transport and organism exposure.

In contrast to aquatic systems, few studies have been performed to quantify and characterize micro- and

<sup>a</sup> Department of Crop & Soil Sciences, Washington State University, Pullman, WA 99164, USA. E-mail: flury@wsu.edu

<sup>b</sup> Energy and Environment Directorate, Pacific Northwest National Laboratory, Richland, WA 99352, USA

<sup>c</sup> Environmental Molecular Sciences Laboratory, Pacific Northwest National Laboratory, Richland, WA 99352, USA

<sup>d</sup> Earth and Biological Sciences Directorate, Pacific Northwest National Laboratory, Richland, WA 99352, USA

<sup>e</sup> College of Land and Environment, Shenyang Agricultural University, Shenyang, China

<sup>f</sup> Department of Crop & Soil Sciences, Washington State University, Puyallup, WA 98371, USA

† Electronic supplementary information (ESI) available. See DOI: 10.1039/d0en00309c

nanoplastics in terrestrial systems.<sup>11,12</sup> The few reported studies show evidence of microplastic particles in floodplain soils,<sup>13</sup> microplastic particles released into rivers as a result of flooding events in suburban and urban soils,<sup>14</sup> microplastic as a vector for metal accumulation in terrestrial invertebrates,<sup>9</sup> and microplastic transport by earthworms<sup>15,16</sup> and collembolan species.<sup>17</sup> Concentrations of plastics reported in floodplain soils can reach up to 55.5 mg kg<sup>-1</sup> soil or 593 particles per kg soil.<sup>13</sup>

Plant roots can take up nanoparticles through the apoplast, through endocytosis across cell membranes,<sup>18,19</sup> and through the endodermis into root vascular tissue by the symplast.<sup>20,21</sup> Symplastic uptake involves movement through root cell membranes, *via* plasmodesmata or endocytosis, and eventually across the endodermis into root xylem.<sup>20,22–24</sup> The basal size exclusion limit of plasmodesmata is thought to be 3–4 nm,<sup>25</sup> though variability exists depending on plant type and developmental stage.<sup>26</sup> The pore size of plasmodesmata can increase considerably through dilation or structural changes, and this can allow larger particles to pass into cells.<sup>25</sup> An exact size exclusion limit of plasmodesmata is thus difficult to define as plasmodesmata size changes due to change in the chemical environment.<sup>27,28</sup> Further, size exclusion capabilities are less well-developed when cells are undergoing cell death or are damaged. Diameters of plasmodesmata considerably larger than the basal size exclusion limit of 3–4 nm have been reported (20–40 nm, <200 nm).<sup>27</sup> Size exclusion limits for nanoparticle uptake by plants are considered to be 40 to 50 nm.<sup>24</sup>

Several studies have shown plant uptake of nanoparticles. CeO<sub>2</sub> nanoparticles (25–42 nm) were found in both xylem and phloem of cucumber (*Cucumis sativus*) exposed hydroponically for 3 days to nanoparticle concentrations of 200 or 2000 mg L<sup>-1</sup>,<sup>29</sup> in leaves and roots of wheat (*Triticum aestivum*) exposed hydroponically for 7 days to nanoparticle concentrations of 20 mg L<sup>-1</sup>,<sup>30</sup> and in leaves and roots of soybeans (*Glycine max* L. Merr.) exposed for 30 days in sandy soil at nanoparticle concentrations of 500 mg kg<sup>-1</sup> dry sand.<sup>31</sup> Pristine and sulfidized silver nanoparticles (42–100 nm) were found in 2 week old, hydroponically grown cowpea (*Vigna unguiculata* L. Walp) and wheat (*T. aestivum*) exposed to 0.6 mg L<sup>-1</sup> metallic silver nanoparticles and 6.0 mg L<sup>-1</sup> sulfidized silver nanoparticles.<sup>32</sup> Similar results were observed for 3 week old, hydroponically grown wheat.<sup>33</sup> Gold nanoparticles (12 nm) were found in Arabidopsis (*Arabidopsis thaliana*) root cells<sup>34</sup> after 10 days exposure at 10 mg L<sup>-1</sup>. Titanium oxide nanoparticles (19–37 nm) were found in rice (*Oryza sativa* L.) roots and shoots, but not in leaf tissue after 24 hour hydroponic exposure at 5 and 50 mg L<sup>-1</sup> until the first leaf growth stage.<sup>35</sup>

Carbon nanotubes are also taken up by plant roots and translocated to different tissue. Single-walled carbon nanotubes (1–4 nm outer diameter (OD), 5–30 nm length) accumulated in corn (*Zea mays* L.) roots exposed in soil for 40 days at concentrations of 10 and 100 mg kg<sup>-1</sup>, and were also seen in stems and leaves.<sup>36</sup> Multi-walled carbon

nanotubes (10–150 nm OD) were found in 22 day old, hydroponically grown wheat (*T. aestivum*) and rapeseed (*Brassica napus*) exposed for 7 days at 1000 mg L<sup>-1</sup>.<sup>37</sup> Multi-walled carbon nanotubes (11 nm OD, ≈1000 nm length) were found in red spinach (*Amaranthus tricolor* L.) roots and leaves exposed hydroponically for 15 days to carbon nanotube concentrations from 0–1000 mg L<sup>-1</sup>.<sup>38</sup> Cañas *et al.*<sup>39</sup> observed single-walled carbon nanotubes (≈8 nm OD, 100–1000 nm length) adsorbing to root cells of corn (*Z. mays*), carrot (*Daucus carota*), onion (*Allium cepa*), tomato (*Lycopersicon esculentum*), cucumber (*C. sativus*), lettuce (*Lactuca sativa*), and cabbage (*Brassica oleracea*), but no nanotubes were found inside root tissue.<sup>39</sup>

While there is ample evidence for plant uptake of metal and carbon-tube nanoparticles, little data exist on whether plastic nano- and microparticles are taken up by plant roots and distributed through the plant tissue. From germination experiments on filter papers, there is evidence that plastic particles can accumulate at seeds and root hairs and block pores,<sup>40</sup> and tobacco BY-2 cell cultures have shown uptake of 20 and 40 nm fluorescent, polystyrene spheres by endocytosis.<sup>18</sup> However, whether plastic particles can be taken up by intact roots is not known. Here, we investigate the uptake and interaction of negatively charged, spherical, polystyrene micro- and nanoparticles with roots of Arabidopsis and wheat.

## 2 Materials and methods

### 2.1 Nano- and microspheres

Two different sizes of fluorescent, carboxylate-modified polystyrene nano- and microspheres were used: 40 nm and 1 μm diameter (ThermoFisher Scientific, USA). We hypothesized that the first (40 nm) could be taken up, and the second (1 μm) cannot based on plasmodesmata size on previous reports on nanoparticle uptake by roots. Excitation and emission wavelengths for the spheres were 505 and 515 nm, respectively. Characteristics of the polystyrene spheres are given in Table 1.

### 2.2 Plant experiments

Arabidopsis (*A. thaliana* ecotype Columbia) and soft white spring wheat cv. Louise (*Triticum aestivum*) were used. Arabidopsis and wheat were chosen as representatives of dicots and monocots, respectively. Arabidopsis is often used as a model for dicot root systems. Roots of cereals like wheat are more complex and have more cortical cell layers compared with Arabidopsis, which has only a single cell layer.<sup>41</sup> Arabidopsis and wheat seeds were surface sterilized in 20% bleach, Triton X-100 (Sigma-Aldrich) solution for 10 minutes, rinsed three times with sterile, distilled water, added to a 70% ethanol solution for two minutes, and rinsed again four times in sterile, distilled water. Both Arabidopsis and wheat seeds were stored in distilled water at (4 °C) for three days to allow them to synchronize germination.

**Table 1** Characteristics of polystyrene nano- and microspheres. Stock concentration of the spheres was  $1.44 \times 10^{14} \text{ n L}^{-1}$ . Polystyrene spheres are surface modified with carboxylic acid groups (ThermoFisher Scientific, USA). Electrophoretic mobility of the spheres in distilled water was measured using a zeta potential analyzer (ZetaPALS, Brookhaven Instruments Corp., Holtsville, NY). Data are mean and standard deviations of 10 measurements

Particle diameter (nm)	Color	Excitation (nm)	Emission (peak) (nm)	Zeta potential (mV)	Electrophoretic mobility ( $\mu\text{m s}^{-1}/(\text{V cm}^{-1})$ )	Lot nr.
40	Green	505	515	$-36.1 \pm 3.5$	$-2.83 \pm 0.28$	F8795
1000	Green	505	515	$-22.8 \pm 3.2$	$-1.79 \pm 0.25$	F8888

All plants were grown in sterile Petri dishes (Fisherbrand, 08-757-11A or -12, Fisher Scientific) with 25 mL growth medium including 0.5% agar (Phytigel, Sigma-Aldrich) and one-fourth strength Hoagland solution.<sup>42</sup> Nano- or microspheres were mixed with the growth media, and then heated on a hot plate to 80 °C before the agar was added. The concentration of plastic spheres in the growth media was  $0.029 \text{ g L}^{-1}$  or  $8.3 \times 10^{11} \text{ n mL}^{-1}$  for the 40 nm spheres, and  $0.029 \text{ g L}^{-1}$  or  $5.3 \times 10^7 \text{ n mL}^{-1}$  for the 1  $\mu\text{m}$  spheres. Growth media without spheres were prepared as a control.

The growth media with the beads was then autoclaved 20 minutes at 121 °C. Wheat seeds (10 seeds) and Arabidopsis seeds (16 seeds) were sown in Petri dishes containing autoclaved media for each treatment, in a laminar flow hood, under sterile conditions. Petri dishes were closed and sealed. Plants were grown to the 1–2 leaf developmental stage (5 days for wheat, 12–15 days for Arabidopsis) under a day/night cycle of 16/8 h with temperatures of 22 °C/18 °C day/night in a growth chamber. The plants were then fixed by adding 10 mL of 4% paraformaldehyde to the Petri dish to cover the plants, then placed under vacuum for 2 hours, and stored at 4 °C until imaging. Each of the three treatments (40 nm, 1  $\mu\text{m}$ , and no spheres) were replicated three times and eight plants from each treatment were imaged. Details on experimental treatments are summarized in Table 2, and images of plants are shown in Fig. S1.†

To check whether the vacuum fixation step would cause experimental artifacts, some of the plants were not fixed with paraformaldehyde but rather directly imaged. In addition, some plants were grown in agar without fluorescent nano- or microspheres, but the fluorescent spheres were added during the fixation step.

### 2.3 Confocal microscopy

Plant samples were examined with laser scanning confocal microscopy (Zeiss LSM 710, Jena, Germany) to determine the

presence of fluorescent polystyrene nano- and microspheres. Plant roots were imaged inside the agar by cutting rectangles around the plants, and placing the agar embedded plants on glass microscopy slides. Eight plants from each treatment were used for data collection, and each treatment was replicated three times. Confocal microscopy images were taken at the pre-differentiated zone of the root (root tip), 1–2 mm below the hypocotyl, and 2–3 mm above the hypocotyl–root intersection. Z-stack images acquired at each location allowed for visualization of the root structure. All fixed plant samples were counter-stained by adding calcofluor white staining solution ( $0.5 \text{ mg mL}^{-1}$ , Sigma-Aldrich) onto the agar for sufficient time to allow the stain to move through agar and stain the plant cells walls (15–20 minutes). For those samples that were imaged right after the 1–2 leaf developmental stage and without the fixation step, plants were pulled out from the agar and dipped into a propidium iodide staining solution ( $0.1 \text{ mg mL}^{-1}$ , ThermoFisher) for 30 minutes of staining before imaging on the confocal microscope. Further details on confocal imaging are given in ESI† (section S1 and S2, Table S1 and Fig. S2).

We also examined cross-sections of calcofluor stained wheat roots. After imaging the full root tips, three wheat root samples from each treatment were pulled from the agar and placed in optimal cutting temperature (O.C.T) embedding medium (Tissue Plus O.C.T Compound, Fisher HealthCare), frozen at  $-20 \text{ °C}$  and then cross-sectioned to a thickness of 20  $\mu\text{m}$  in the embedding media using a Cryostat (CryoStar NX70, ThermoFisher Scientific). Confocal imaging was done as described above.

The polystyrene particles were tested for stability of the fluorescence across various pH they may encounter in the environment immediately around the root surface. No effect of pH on fluorescence was found. Further, heating and autoclaving did not substantially affect the fluorescence or size and shape of the beads (see ESI† section S2, Fig. S3 and S4).

**Table 2** Summary of experimental treatments. Concentration of plastic in growth media by mass was  $0.029 \text{ g L}^{-1}$

Treatments	Diameter of microspheres (nm)	Concentration of spheres ( $\text{n mL}^{-1}$ )	Plant species	Growth time (days)	Parts imaged
Control	—	0	Arabidopsis	12–15	Root tip,
40 nm	40	$8.3 \times 10^{11}$		12–15	Hypocotyl
1 $\mu\text{m}$	1000	$5.3 \times 10^7$		12–15	(Above/below)
Control	—	0	Wheat	5	Root tip,
40 nm	40	$8.3 \times 10^{11}$		5	Hypocotyl
1 $\mu\text{m}$	1000	$5.3 \times 10^7$		5	(Above/below)

## 2.4 Pyrolysis GC-MS

Arabidopsis plants and wheat roots ( $n = 3$ ), including the tip, from each treatment were washed three times using phosphate-buffered saline (PBS) with 1% Triton X-100, vortexing for 30 seconds, and sonication for 5 minutes. Washed plant material was completely dried, weighed, and analyzed by pyrolysis GC-MS. Polystyrene thermal degradation products were used to indicate uptake of plastic inside the roots. Negative control plant roots and polystyrene spheres were also analyzed for thermal degradation products at the pyrolysis settings used. More details on the pyrolysis GC-MS are given in the ESI† (section S3, Table S2).

## 3 Results and discussion

### 3.1 Association of nano- and microspheres with roots

All eight plants for each of the three replicates showed the same experimental results, and we therefore only present selected images in the following sections.

Confocal microscopy of the pre-differentiated zone (root tips) in growth media showed no evidence for uptake of nano- or microspheres in Arabidopsis or wheat roots beyond root cap cells (Fig. 1 and 2). The images show root epidermal cells with calcofluor counter-staining in the absence (Fig. 1A and 2A) and presence (Fig. 1B and C and 2B and C) of fluorescent spheres. In both plant species, the 40 nm and 1  $\mu\text{m}$  fluorescent spheres accumulated on the outside of the root cells. Fig. 1C and 2C show the 1  $\mu\text{m}$  plastic microspheres on the surface of root epidermal cells. Individual 1  $\mu\text{m}$  polystyrene microspheres were more easily imaged, but similar results were obtained for the nanospheres. Orthogonal images (Fig. 1 and 2, right column) show the localization and aggregation of fluorescent spheres on the surface of the root cells. The 40 nm and 1  $\mu\text{m}$  spheres were restricted to the root surface and did not extend into the internal root structure, through either apoplastic or symplastic pathways, indicating no active uptake of the plastic particles by living cells.

There is some evidence for the presence of the 40 nm polystyrene spheres inside root cap cells (Fig. 1B and 2B). Aggregates of 40 nm fluorescent spheres (white arrows) are visible on the surface of root epidermal cells, and inside the root border cells, or root cap (red arrows). However, no spheres are visible internal to the active root cells and deeper into the root vascular tissue. The 1  $\mu\text{m}$  particles are visible on the surface of the root cells only, but not inside root cap cells (Fig. 1C and 2C). The right column of Fig. 1 and 2 are orthogonally projected images in the  $X$ - $Y$ ,  $X$ - $Z$  and  $Y$ - $Z$  directions. In the  $X$ - $Z$  and  $Y$ - $Z$  panels, calcofluor stain (blue color) shows the cells walls and any fluorescence interior to that in the  $z$ -direction indicates uptake into the root cap cells. Arrows show particles inside cells (red) and on the cell surface (white).

To check whether the 40 nm fluorescent spheres inside root cap cells were an artifact of the fixation technique, Arabidopsis and wheat roots that were grown in agar with no

plastic spheres, but had 40 nm fluorescent spheres introduced during the fixation step. These images also showed some evidence of plastic inside the root cap cells (Fig. 3A, red arrows for Arabidopsis). However, live cell imaging, without fixation and using a propidium iodide counter-stain, did not show any fluorescent spheres inside live, propidium iodide impermeable root cap cells (Fig. 3B, white arrows) or dead, propidium iodide permeable root cap cells (Fig. 3C, white arrows). The presence of the 40 nm spheres in the root cap cells (Fig. 1A and 2A, red arrows) is, therefore, likely an artifact of our fixation technique, where root cap border cells in the process of programmed cell death (PCD) and sloughing off are more permeable to nanoplastic particles, and fixation drove the 40 nm fluorescent particles into the dead cells. Additionally, Fig. 3C shows that the accumulation of the fluorescent, polystyrene nanoparticles at the surface of the root tip was not an artifact of the fixation.

Root cap cells are short-lived cells with a high turn-over that help with regulating root directional growth and protect the root stem cell niche. Root cap tissue is categorized as central columella (COL) tissue around the root apex and lateral root cap (LRC) tissue on the periphery extending up towards the root epidermis around the meristem. In Arabidopsis, LRC cells undergo cell death and are released as they age, moving towards the apex where they are finally released in a "packet".<sup>43,44</sup> Wheat LRC cells detach and are released individually.<sup>43</sup> Fig. 4 shows accumulation of 1  $\mu\text{m}$  polystyrene spheres at discarded root cap cells. Nanoparticle interaction with, and even accumulation around, root cap cells has also been shown for gold nanoparticles in Arabidopsis, and uptake of negatively-charged nanoparticles into the root cells has been observed.<sup>34</sup> However, in our study, no uptake of plastic beyond the border cells was observed.

Confocal images with roots in the agar medium show how growing roots push through the medium, displacing the polystyrene spheres and collecting them at the root tip (Fig. 1B and 2C). In Fig. 4, accumulation of polystyrene spheres on discarded root cap cells of Arabidopsis can be seen. This supports the idea that the developmental function of the root cap is a protective barrier for the stem cell niche and root meristem, as it appears that the plastic particles are shielded by the root cap cells (Fig. 4). As part of their protective function, root cap cells excrete mucilage and other exudates as a first line of defense against toxic chemicals and mechanical stress, while dissolving nutrients and aggregating soil particles.<sup>27,45–47</sup> Detached border-like cells of Arabidopsis and associated mucilage have been reported to trap positively-charged, and also negatively-charged, gold nanoparticles.<sup>34</sup> The same mechanism may operate for the negatively-charged plastic particles in our study.

Fig. 5 shows that, even after rigorous washing prior to the GC-MS analysis, polystyrene spheres were still attached to the roots. This suggests that plastic beads were not just pushed aside by the growing roots, but rather were firmly attached to the root surface.

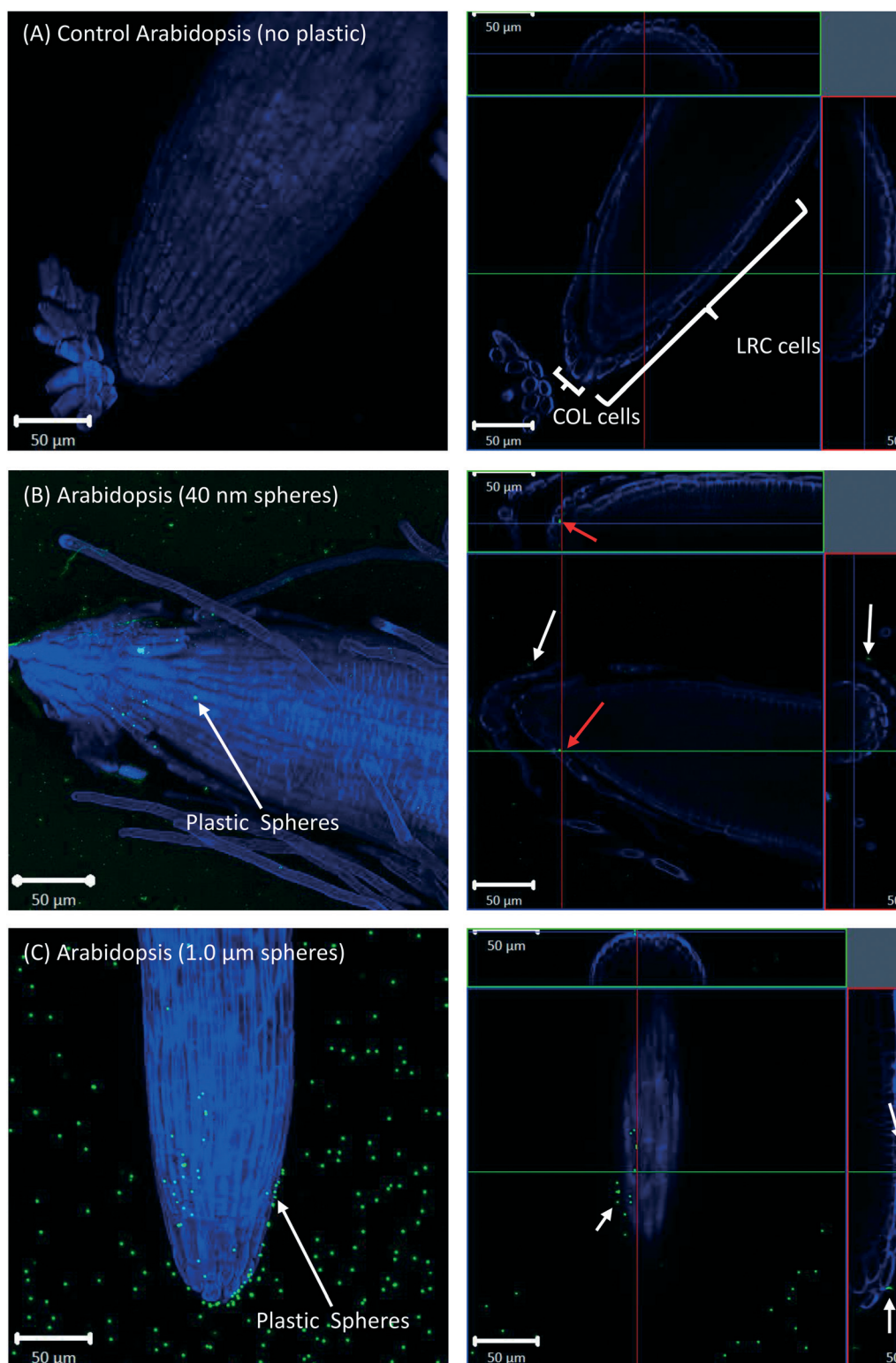


**Fig. 1** Images of Arabidopsis root tips with calcofluor stain (410–497 nm detection channel) and fluorescent spheres (493–582 nm detection channel) tracks overlaid. Maximum intensity projections (left column) of plants grown in (A) control media, (B) 40 nm fluorescent polystyrene spheres, and (C) 1  $\mu\text{m}$  fluorescent polystyrene spheres. The right column shows orthogonally projected images in the X–Y, X–Z, and Y–Z directions. White arrows highlight particles on surface of the root cells, red arrows highlight particles internal to root cells. COL: central columella; LRC: lateral root cap.

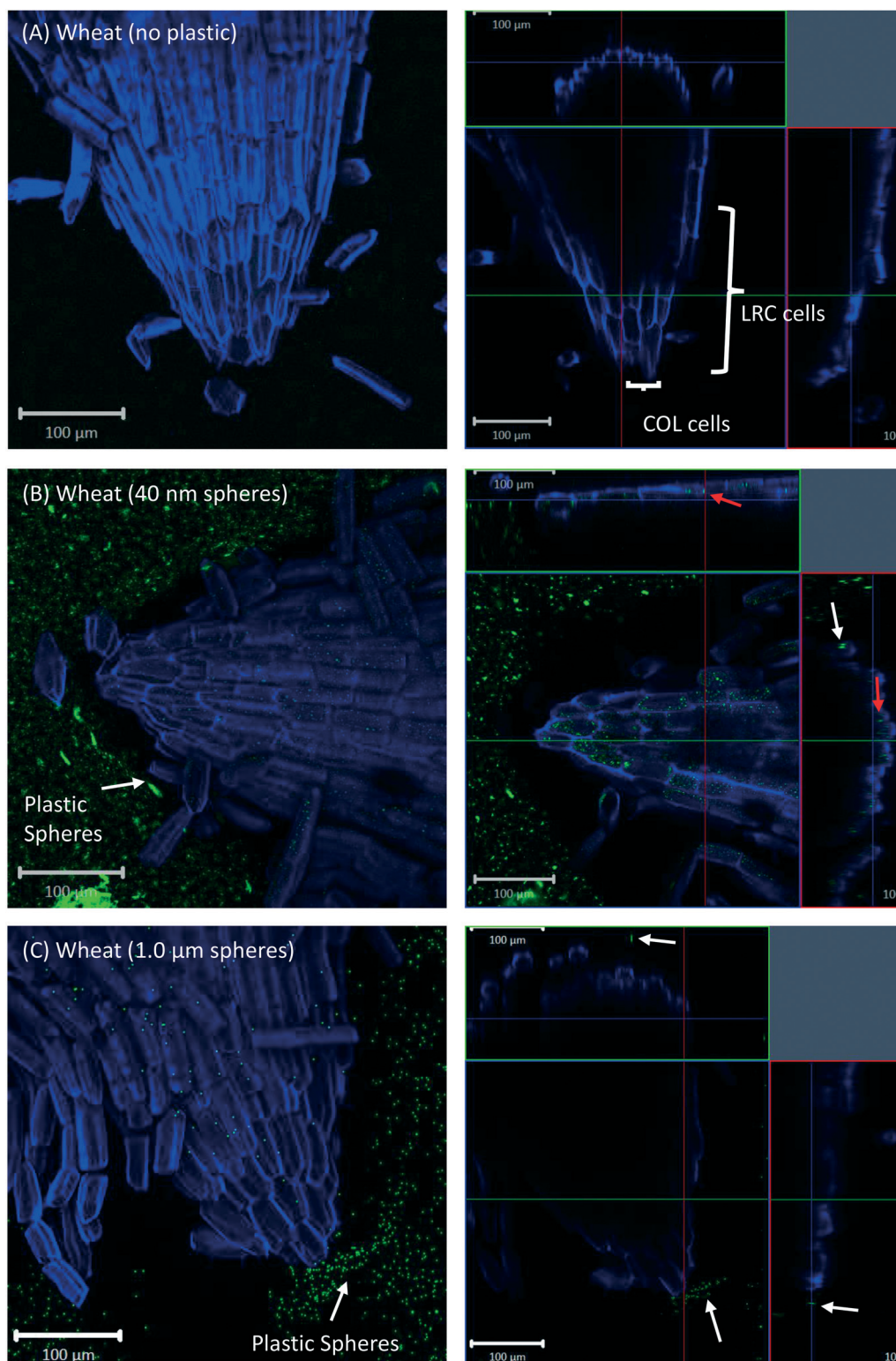


**Fig. 2** Images of wheat root tips with calcofluor stain (410–497 nm detection channel) and fluorescent spheres (493–582 nm detection channel) tracks overlaid. Maximum intensity projections (left column) of plants grown in (A) control media, (B) 40 nm fluorescent polystyrene spheres, and (C) 1 μm fluorescent polystyrene spheres. The right column shows orthogonally projected images in the X–Y, X–Z, and Y–Z directions. White arrows highlight particles on surface of the root cells, red arrows highlight particles internal to root cells. COL: central columella; LRC: lateral root cap.

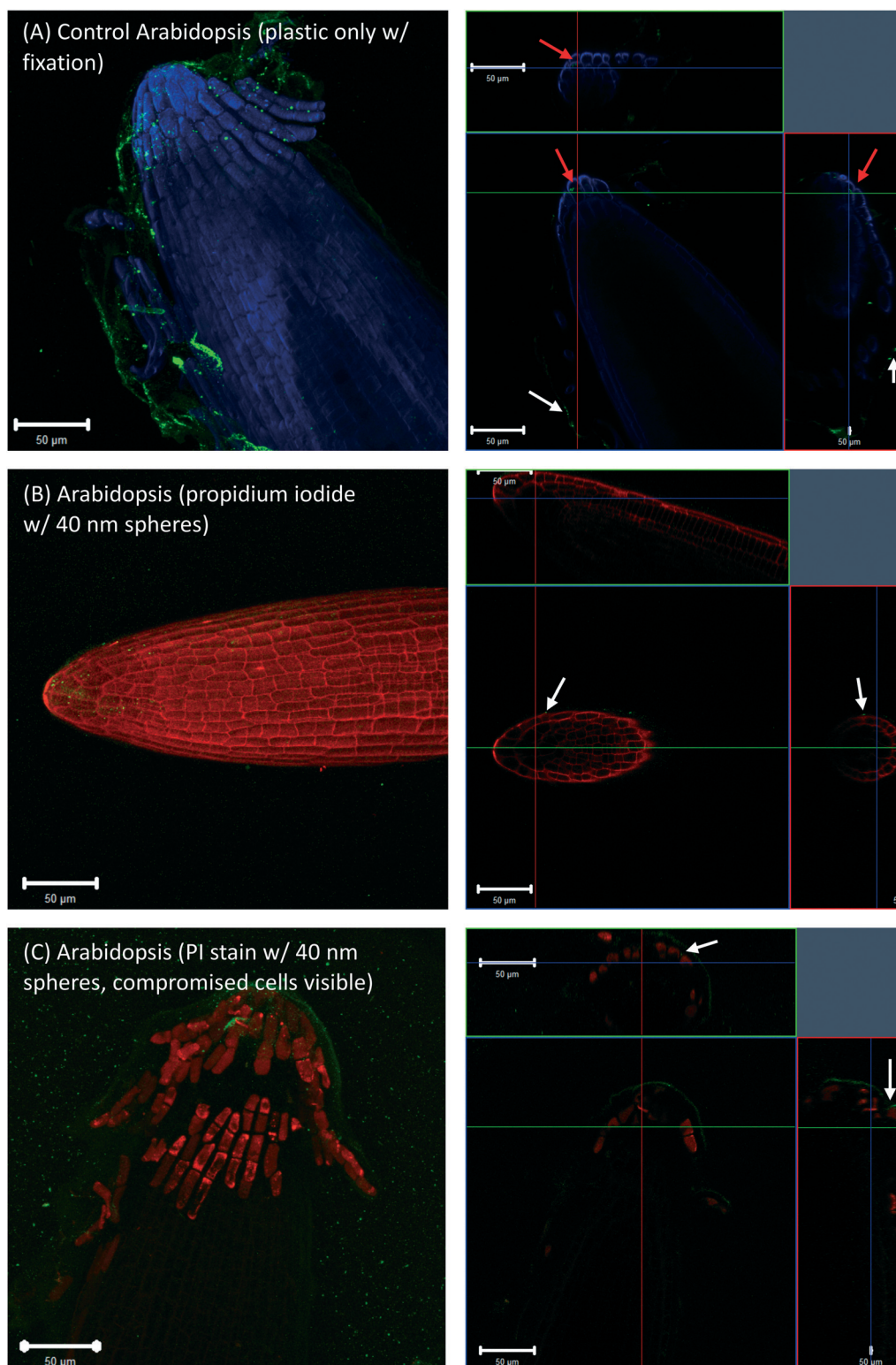


**Fig. 3** Images of Arabidopsis root tips. (A) Roots grown in agar without plastic spheres present, but 40 nm spheres were introduced during the fixation procedure. Roots were pulled out from agar prior to imaging. (B) Propidium iodide-stained roots grown in agar containing 40 nm fluorescent beads show no movement of the beads into root cap cells. (C) Root cap cells that have already undergone cell death are shown as bright red due to the propidium iodide entering the cell and staining lysed DNA and RNA. The right column shows orthogonally projected images in the X-Y, X-Z, and Y-Z directions. White arrows highlight particles on surface of the root cells, red arrows highlight particles internal to root cells.

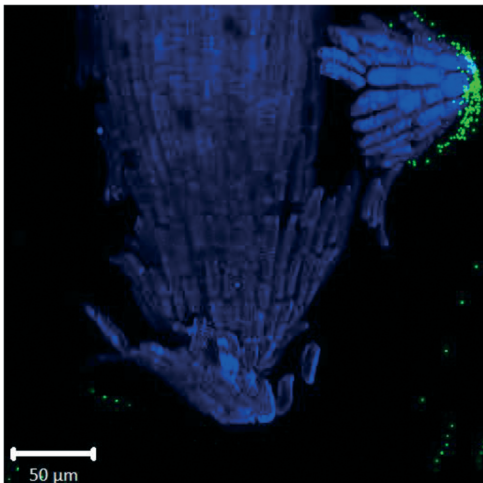


Fig. 4 Confocal images of Arabidopsis root tip showing 1  $\mu\text{m}$  fluorescent polystyrene spheres accumulated around discarded root cap cells.

Cross-sections of root tips confirmed that polystyrene spheres were not actively taken up by the roots (Fig. S5†). The 40 nm spheres, but not the 1  $\mu\text{m}$  spheres, were observed inside root cap cells (Fig. S5C and D†), but based on our control experiments, we consider the presence of beads inside the root cap cells an experimental artifact of the fixation technique. Confocal images of Arabidopsis and wheat plants about 2 mm above and below the hypocotyl region show no evidence for the presence of polystyrene nano- and microspheres inside any root or shoot cells; however, there is evidence of association of polystyrene spheres with the surface of root hairs (Fig. 6).

Surface charge of particles is an important parameter controlling how nanoparticles interact with root cells. As the root surface cells are negatively charged, positively-charged nanoparticles will adhere by electrostatic forces to the root

cells while negatively-charged particles will be repelled. Experiments in hydroponic systems with particles of different surface charge have shown that positively-charged nanoparticles mostly attach to or are retained in root cells, but are not readily translocated to leaves, while neutral and negatively-charged particles are more readily transferred into the interior of the plants and can be translocated to the leaves.<sup>30,48,49</sup> For negatively-charged gold nanoparticles, it was reported that their negative surface charge minimized interaction with cell walls and led to a low amount of uptake into the root cells.<sup>48</sup>

While uptake of nanoparticles by plants is more likely to occur in a hydroponic system, such uptake has also been observed when plants were grown in gels. Avellan *et al.*<sup>34</sup> grew *A. thaliana* in a Phytigel containing gold nanoparticles, and observed uptake of negatively-charged nanoparticles into the apoplast, but positively-charged nanoparticles were trapped by the root cap cells and in the mucilage. Our experiments, also done with roots growing in gel, provided no evidence for uptake and translocation of negatively-charged polystyrene nanoparticles. It may be possible that in our experiments a small, non-detectable amount of polystyrene nanoparticles may have entered into the interior of root cells, but overall the interaction of polystyrene nanoparticles was confined to the root surface and cap cells. The size of the nanoparticles may explain in part the absence of root uptake in our study: our polystyrene particles (40 nm) were larger than the gold particles (12 nm) used by Avellan *et al.*<sup>34</sup>

### 3.2 Plant vigor

No obvious differences in plant health (seed germination rate, root length, or plant height) were observed between treatments (Fig. S1†). Recent studies have reported negative impacts of microplastic particles in the soil on plant growth.<sup>50–53</sup> While some of these negative impacts were

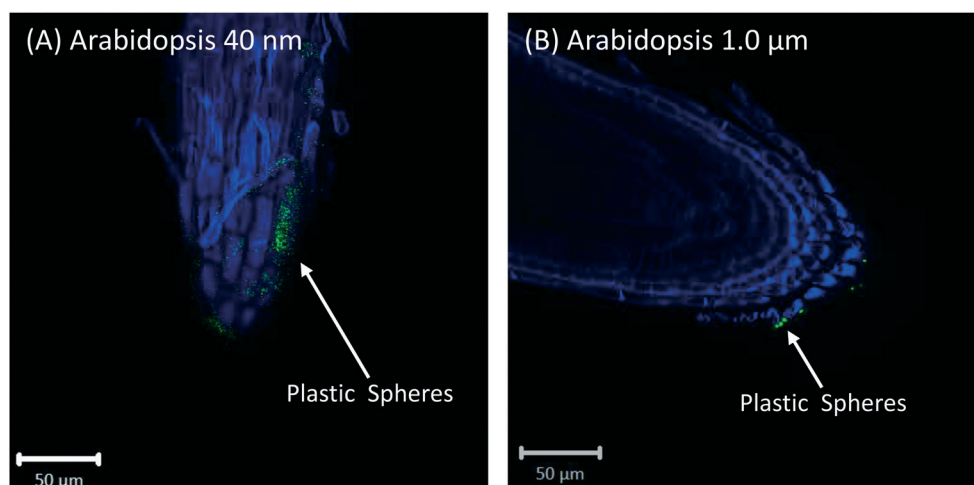
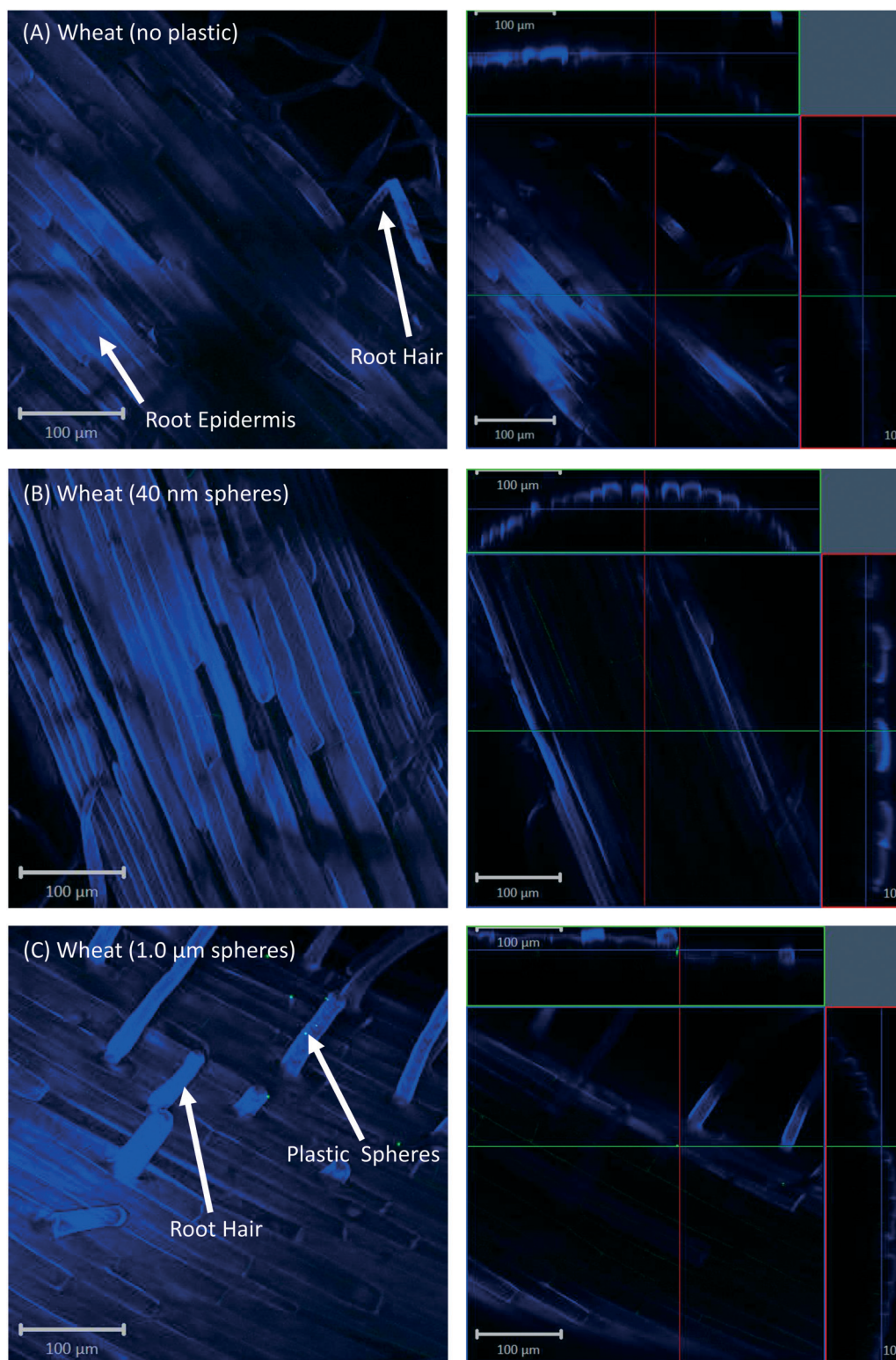


Fig. 5 Arabidopsis root images of the pre-differentiated zone of the root after washing. (A) 40 nm spheres, (B) 1.0  $\mu\text{m}$  spheres. These images show that there were still fluorescent spheres left on the surface of the root after washing.





**Fig. 6** Images of wheat root 2 mm below hypocotyl region. All images show root epidermal cells with calcofluor staining. Image C shows evidence for surface interactions (see arrows) with 1 μm polystyrene spheres, but not uptake. The right column shows orthogonally projected images in the X-Y, X-Z, and Y-Z directions, with cross-hairs placed on root surface for negative control treatment (A), inside root cells for 40 nm treatment (B), and over fluorescent spheres in (C). No plastic particles spheres were observed in the hypocotyl region for the negative control or the 40 nm treatment.

attributed to changes in soil biophysical parameters like aggregate stability, water holding capacity, and pH, it is conceivable that plastics have also direct negative impacts on plant growth through interactions with the root surfaces.

### 3.3 Pyrolysis GC-MS

The pyrolysis GC-MS analysis shows a strong styrene peak for the polystyrene sphere standards (Fig. S6†). However, small styrene peaks were also observed for both wheat and Arabidopsis roots grown in the absence of polystyrene spheres (negative controls). Others also reported the formation of styrene as a pyrolysis degradation product of plant material.<sup>54,55</sup> We observed styrene chromatography peaks in both wheat and Arabidopsis roots grown in the presence of 40 nm and the 1  $\mu\text{m}$  polystyrene spheres (Fig. S6 and S7†). In addition, we observed two other polystyrene degradation products (3-butene-1,3-diyldibenzene and 5-hexene-1,3,5-triyltribenzene), in both the control and polystyrene-exposed plants. Therefore, we were not able to identify polystyrene particles in the plant roots with pyrolysis GC-MS (see ESI† section 3 for further discussion).

Pyrolysis GC-MS has been used to identify microplastics in environmental samples, including seawater, beach sediments, and marine organisms.<sup>56</sup> The detection limit for polystyrene with this technique has been reported to be 0.003  $\mu\text{g}$  per pyrolysis analysis cup.<sup>56</sup> This would correspond to 5450 of 1  $\mu\text{m}$  polystyrene particles or  $8.5 \times 10^7$  of 40 nm polystyrene particles. The pyrolysis GC-MS technique can only detect large numbers of polystyrene particles inside plant roots. The detection limits with confocal microscopy are much lower, as a single 1  $\mu\text{m}$  polystyrene particle can clearly be identified and multiple 40 nm polystyrene particle are visible. Moreover, confocal microscopy also allows spatial resolution of the location of the particles.

## 4 Conclusions

Previous research with hydroponic plant cultures has shown that nanoparticles (diameter 10 to 100 nm) to be can be taken up by roots and be translocated in the plant tissue. Hydroponic systems are conducive for nanoparticle uptake by plants because the nanoparticles are free to move, and no sites other than root surface are available for the nanoparticles to attach. While studies with hydroponic systems demonstrate the potential for nanoparticle uptake, this does not necessarily mean that nanoparticle uptake also occurs in real soils. In soils, nanoparticles are much less mobile and can attach to organic matter and mineral surfaces. Studies with plants grown in solid media, such as gels or soil are less common, but also have shown root uptake of nanoparticles.<sup>31,34,36</sup> Our results with plants grown in gel show no evidence for active uptake of nano- and microsized polystyrene spheres (40 nm) in Arabidopsis and wheat roots, but accumulation of the plastic particles at the root surface, particularly at the root tip. It may be possible that the plastic particles used in our study were too large to

be taken up, and smaller particles could possibly be taken up by roots. Translocation of ions and particles across cell membranes often requires specific promoters,<sup>25,27</sup> and many transition metal transporters are known.<sup>57</sup> It is thus conceivable that metallo-compounds in the rhizosphere could be taken up by plants whereas plastics are not.

## Author contributions

SET, CIP, KAS, ZW, MF conceived and designed research; SET, MF led overall study; SET, CIP, KAS, MF wrote manuscript and analyzed data; DH and WBC performed confocal microscopy; YMK assisted with pyrolysis GC-MS; all co-authors contributed to data interpretation and editing.

## Conflicts of interest

There are no conflicts to declare.

## Acknowledgements

A portion of the research was performed using EMSL (user projects 49732 and 51323), a DOE Office of Science User Facility sponsored by the Office of Biological and Environmental Research. We thank Pubudu Handakumbura at PNNL for her help and advice with plant growth, and Jonathan Lomber at Washington State University's Biosystems Engineering Analytical Chemistry Laboratory for assistance with pyrolysis GC-MS data collection. Funding was provided by the WSU-PNNL Distinguished Graduate Student Fellowship, the USDA/NIFA Hatch project 1014527, the USDA/NIFA Hatch W3188 Multi-State Project, and under the Laboratory Directed Research and Development Program at Pacific Northwest National Laboratory, a multiprogram national laboratory operated by Battelle for the U.S. Department of Energy.

## References

- 1 C. M. Rochman, S. M. Kross, J. B. Armstrong, M. T. Bogan, E. S. Darling, S. J. Green, A. R. Smyth and D. Verissimo, Scientific Evidence Supports a Ban on Microbeads, *Environ. Sci. Technol.*, 2015, **49**, 10759–10761.
- 2 L. Nizzetto, M. Futter and S. Langaas, Are Agricultural Soils Dumps for Microplastics of Urban Origin?, *Environ. Sci. Technol.*, 2016, **50**, 10777–10779.
- 3 M. Cole, P. Lindeque, C. Halsband and T. S. Galloway, Microplastics as contaminants in the marine environment: A review, *Mar. Pollut. Bull.*, 2011, **62**, 2588–2597.
- 4 S. Allen, D. Allen, V. R. Phoenix, G. Le Roux, P. D. Jiménez, A. Simonneau, S. Binet and D. Galop, Atmospheric transport and deposition of microplastics in a remote mountain catchment, *Nat. Geosci.*, 2019, **12**, 339–344.
- 5 M. A. Browne, A. Dissanayake, T. S. Galloway, D. M. Lowe and R. C. Thompson, Ingested microscopic plastic translocates to the circulatory system of the Mussel, *Mytilus edulis* (L.), *Environ. Sci. Technol.*, 2008, **42**, 5026–5031.

- 6 D. Brennecke, B. Duarte, F. Paiva, I. Caçador and J. Canning-Clode, Microplastics as vector for heavy metal contamination from the marine environment, *Estuarine, Coastal Shelf Sci.*, 2016, **178**, 189–195.
- 7 J. Liu, Y. Ma, D. Zhu, T. Xia, Y. Qi, Y. Yao, X. Guo, R. Ji and W. Chen, Polystyrene nanoplastics-enhanced contaminant transport: role of irreversible adsorption in glassy polymeric domain, *Environ. Sci. Technol.*, 2018, **52**, 2677–2685.
- 8 O. S. Alimi, J. Farner Budarz, L. M. Hernandez and N. Tufenkji, Microplastics and nanoplastics in aquatic environments: aggregation, deposition, and enhanced contaminant transport, *Environ. Sci. Technol.*, 2018, **52**, 1704–1724.
- 9 M. E. Hodson, C. A. Duffus-Hodson, A. Clark, M. T. Prendergast-Miller and K. L. Thorpe, Plastic bag derived-microplastics as a vector for metal exposure in terrestrial invertebrates, *Environ. Sci. Technol.*, 2017, **51**, 4714–4721.
- 10 H. Lee, W. J. Shim and J.-H. Kwon, Sorption capacity of plastic debris for hydrophobic organic chemicals, *Sci. Total Environ.*, 2014, **470–471**, 1545–1552.
- 11 M. Bläsing and W. Amelung, Plastics in soil: Analytical methods and possible sources, *Sci. Total Environ.*, 2018, **612**, 422–435.
- 12 A. A. Horton, A. Walton, D. J. Spurgeon, E. Lahive and C. Svendsen, Microplastics in freshwater and terrestrial environments: Evaluating the current understanding to identify the knowledge gaps and future research priorities, *Sci. Total Environ.*, 2017, **586**, 127–141.
- 13 M. Scheurer and M. Bigalke, Microplastics in Swiss Floodplain Soils, *Environ. Sci. Technol.*, 2018, **52**, 3591–3598.
- 14 R. Hurley, J. Woodward and J. J. Rothwell, Microplastic contamination of river beds significantly reduced by catchment-wide flooding, *Nat. Geosci.*, 2018, **11**, 251–257.
- 15 E. Huerta Lwanga, H. Gertsen, H. Gooren, P. Peters, T. Salánki, M. van der Ploeg, E. Besseling, A. A. Koelmans and V. Geissen, Microplastics in the terrestrial ecosystem: Implications for *Lumbricus terrestris* (Oligochaeta, Lumbricidae), *Environ. Sci. Technol.*, 2016, **50**, 2685–2691.
- 16 M. C. Rillig, L. Ziersch and S. Hempel, Microplastic transport in soil by earthworms, *Sci. Rep.*, 2017, **7**, 1362, DOI: 10.1038/s41598-017-01594-7.
- 17 S. Maaß, D. Daphi, A. Lehmann and M. C. Rillig, Transport of microplastics by two collembolan species, *Environ. Pollut.*, 2017, **225**, 456–459.
- 18 V. Bandmann, J. D. Müller, T. Köhler and U. Homann, Uptake of fluorescent nano beads into BY2-cells involves clathrin-dependent and clathrin-independent endocytosis, *FEBS Lett.*, 2012, **586**, 3626–3632.
- 19 C. Craddock and Z. Yang, Endocytic signaling pathways in leaves and roots; same players different rules, *Front. Plant Sci.*, 2012, **3**, 219.
- 20 D. K. Tripathi, S. Singh, S. Singh, R. Pandey, V. P. Singh, N. C. Sharma, S. M. Prasad, N. K. Dubey and D. K. Chauhan, An overview on manufactured nanoparticles in plants: Uptake, translocation, accumulation and phytotoxicity, *Plant Physiol. Biochem.*, 2017, **110**, 2–12.
- 21 J. Li, R. V. Tappero, A. S. Acerbo, H. Yan, Y. Chu, G. V. Lowry and J. M. Unrine, Effect of CeO<sub>2</sub> nanomaterial surface functional groups on tissue and subcellular distribution of Ce in tomato *Solanum lycopersicum*, *Environ. Sci.: Nano*, 2019, **6**, 273–285.
- 22 X. Ma, J. Geiser-Lee, Y. Deng and A. Kolmakov, Interactions between engineered nanoparticles (ENPs) and plants: Phytotoxicity, uptake, and accumulation, *Sci. Total Environ.*, 2010, **408**, 3053–3061.
- 23 M. Xu, E. Cho, T. M. Burch-Smith and P. Zambryski, Plasmodesmata formation and cell-to-cell transport are reduced in decreased size exclusion limit 1 during embryogenesis in Arabidopsis, *Proc. Natl. Acad. Sci. U. S. A.*, 2012, **109**, 5098–5103.
- 24 A. P. de Luque, Interaction of nanomaterials with plants: what do we need for real applications in agriculture?, *Front. Environ. Sci.*, 2017, **5**, 12, DOI: 10.3389/fenvs.2017.00012.
- 25 R. E. Sager and J.-Y. Lee, Plasmodesmata at a glance, *J. Cell Sci.*, 2018, **131**, jcs209346, DOI: 10.1242/jcs.209346.
- 26 K. J. Oparka, A. G. Roberts, P. Boevink, S. S. Cruz, I. Roberts, K. S. Pradel, A. Imlau, G. Kotlizky, N. Sauer and B. Epel, Plasmodesmata at a glance, *Cell*, 1999, **97**, 743–754.
- 27 F. Schwab, G. Zhai, M. Kern, A. Turner, J. L. Schnoor and M. R. Wiesner, Barriers, pathways and processes for uptake, translocation and accumulation of nanomaterials in plants – Critical Review, *Nanotoxicology*, 2015, **10**, 257–278.
- 28 R. Sager and J.-Y. Lee, Plasmodesmata in integrated cell signalling: insights from development and environmental signals and stresses, *J. Exp. Bot.*, 2014, **64**, 6337–6358.
- 29 Y. Ma, X. He, P. Zhang, Z. Zhang, Y. Ding, J. Zhang, G. Wang, C. Xie, W. Luo, J. Zhang, L. Zheng, Z. Chai and K. Yang, Xylem and phloem based transport of CeO<sub>2</sub> nanoparticles in hydroponic Cucumber plants, *Environ. Sci. Technol.*, 2017, **51**, 5215–5221.
- 30 E. Spielman-Sun, E. Lombi, E. Donner, D. Howard, J. M. Unrine and G. V. Lowry, Impact of surface charge on cerium oxide nanoparticle uptake and translocation by wheat (*Triticum aestivum*), *Environ. Sci. Technol.*, 2017, **51**, 7361–7368.
- 31 L. Rossi, W. Zhang, A. P. Schwab and X. Ma, Uptake, Accumulation, and in planta distribution of coexisting cerium oxide nanoparticles and cadmium in *Glycine max* (L.) Merr, *Environ. Sci. Technol.*, 2017, **51**, 12815–12824.
- 32 P. Wang, N. W. Menzies, E. Lombi, R. Sekine, F. P. C. Blamey, M. C. Hernandez-Soriano, M. Cheng, P. Kappen, W. J. G. M. Peijnenburg, C. Tang and P. M. Kopittke, Silver sulfide nanoparticles (Ag<sub>2</sub>S-NPs) are taken up by plants and are phytotoxic, *Nanotoxicology*, 2015, **9**, 1041–1049.
- 33 A. E. Pradas del Real, V. Vidal, M. Carrière, H. Castillo-Michel, C. Levard, P. Chaurand and G. Sarret, Silver nanoparticles and wheat roots: a complex interplay, *Environ. Sci. Technol.*, 2017, **51**, 5774–5782.
- 34 A. Avellan, F. Schwab, A. Masion, P. Chaurand, D. Borschneck, V. Vidal, J. Rose, C. Santaella and C. Levard, Nanoparticle uptake in plants: gold nanomaterial localized in roots of Arabidopsis thaliana by x-ray computed

- nanotomography and hyperspectral imaging, *Environ. Sci. Technol.*, 2017, **51**, 8682–8691.
- 35 Y. Deng, E. J. Petersen, K. E. Challis, S. A. Rabb, R. D. Holbrook, J. F. Ranville, B. C. Nelson and B. Xing, Multiple method analysis of  $\text{TiO}_2$  nanoparticle uptake in rice (*Oryza sativa* L.) Plants, *Environ. Sci. Technol.*, 2017, **51**, 10615–10623.
- 36 A. M. Cano, K. Kohl, S. Deleon, P. Payton, F. Irin, M. Saed, S. A. Shah, M. J. Green and J. E. Cañas Carrel, Determination of uptake, accumulation, and stress effects in corn (*Zea mays* L.) grown in singlewall carbon nanotube contaminated soil, *Chemosphere*, 2016, **152**, 117–122.
- 37 C. Larue, M. Pinault, B. Czarny, D. Georgin, D. Jaillard, N. Bendiab, M. Mayne-L'Hermite, F. Taran, V. Dive and M. Carrière, Quantitative evaluation of multi-walled carbon nanotube uptake in wheat and rapeseed, *J. Hazard. Mater.*, 2012, **227–228**, 155–163.
- 38 P. Begum and B. Fugetsu, Phytotoxicity of multi-walled carbon nanotubes on red spinach (*Amaranthus tricolor* L) and the role of ascorbic acid as an antioxidant, *J. Hazard. Mater.*, 2012, **243**, 212–222.
- 39 J. E. Cañas, M. Long, S. Nations, R. Vadan and L. Dai, Effects of functionalized and nonfunctionalized single-walled carbon nanotubes on root elongation of select crop species, *Environ. Toxicol. Chem.*, 2008, **27**, 1922–1931.
- 40 T. Bosker, L. J. Bouwman, N. R. Brun, P. Behrens and M. G. Vijver, Microplastics accumulate on pores in seed capsule and delay germination and root growth of the terrestrial vascular plant *Lepidium sativum*, *Chemosphere*, 2019, **226**, 774–781.
- 41 S. Smith and I. De Smet, Root system architecture: insights from *Arabidopsis* and cereal crops, *Philos. Trans. R. Soc. Lond., B, Biol. Sci.*, 2012, **367**, 1441–1452.
- 42 D. R. Hoagland and D. I. Arnon, *The water-culture method for the growing of plants without soil*, University of California Berkeley Press, California Agricultural Experiment Station, Circular 347, 1950, p. 347.
- 43 R. P. Kumpf and M. K. Nowack, The root cap: a short story of life and death, *J. Exp. Bot.*, 2015, **66**, 5651–5662.
- 44 R. Karve, F. Suárez-Román and A. S. Iyer-Pascuzzi, The transcription factor NIN-LIKE PROTEIN 7 (NLP7) controls border-like cell release in *Arabidopsis*, *Plant Physiol.*, 2016, **171**, 2101–2111.
- 45 A. G. Bengough and B. McKenzie, Sloughing of root cap cells decreases the frictional resistance to maize (*Zea mays* L.) root growth, *J. Exp. Bot.*, 1997, **48**, 885–893.
- 46 H. P. Bais, S.-W. Park, T. L. Weir, R. M. Callaway and J. M. Vivanco, How plants communicate using the underground information super-highway, *Trends Plant Sci.*, 2004, **9**, 26–32.
- 47 D. H. McNear Jr, The rhizosphere - roots, soil and everything in between, *Nat. Educ. Knowl.*, 2013, **4**, 1.
- 48 Z.-J. Zhu, H. Wang, B. Yan, H. Zheng, Y. Jiang, O. R. Miranda, V. M. Rotello, B. Xing and R. W. Vachet, Effect of surface charge on the uptake and distribution of gold nanoparticles in four plant species, *Environ. Sci. Technol.*, 2011, **46**, 12391–12398.
- 49 H. Li, X. Ye, X. Guo, Z. Geng and G. Wang, Effects of surface ligands on the uptake and transport of gold nanoparticles in rice and tomato, *J. Hazard. Mater.*, 2016, **314**, 188–196.
- 50 Y. Qi, X. Yang, A. Mejia Pelaez, E. Huerta Lwanga, N. Beriot, H. Gertsen, P. Garbeva and V. Geissen, Macro- and micropastics in soil-plant system: Effects of plastic mulch film residues on wheat (*Triticum aestivum*) growth, *Sci. Total Environ.*, 2018, **645**, 1048–1056.
- 51 B. Boots, C. W. Russell and D. S. Green, Effects of microplastics in soil ecosystems: above and below ground, *Environ. Sci. Technol.*, 2019, **53**, 11496–11506.
- 52 A. A. de Souza Machado, C. W. Lau, K. Werner, J. Bergmann, J. B. Bachelier, E. Faltin, R. Becker, A. S. Görlich and M. C. Rillig, Microplastics can change soil properties and affect plant performance, *Environ. Sci. Technol.*, 2019, **53**, 6044–6052.
- 53 M. C. Rillig, A. Lehmann, A. A. de Souza Machado and G. Yang, Microplastic effects on plants, *New Phytol.*, 2019, **223**, 1066–1070.
- 54 L. Chen, X. Wang, H. Yang, Q. Lu, D. Li, Q. Yang and H. Chen, Study on pyrolysis behaviors of non-woody lignins with TG-FTIR and Py-GC/MS, *J. Anal. Appl. Pyrolysis*, 2015, **113**, 499–5070.
- 55 E. Rouches, M.-F. Dignac, S. Zhou and H. Carrere, Pyrolysis-GC-MS to assess the fungal pretreatment efficiency for wheat straw anaerobic digestion, *J. Anal. Appl. Pyrolysis*, 2017, **123**, 409–418.
- 56 L. Hermabessiere, C. Himber, B. Boricaud, M. Kazour, R. Amara, A.-L. Cassone, M. Laurentie, I. Paul-Pont, P. Soudant, A. Dehaut and G. Duflos, Optimization, performance, and application of a pyrolysis-GC/MS method for the identification of microplastics, *Anal. Bioanal. Chem.*, 2018, **410**, 6663–6676.
- 57 M. Gonzalez-Guerrero, V. Escudero, A. Saez and M. Tejada-Jimenez, Transition metal transport in plants and associated endosymbionts: arbuscular mycorrhizal fungi and rhizobia, *Front. Plant Sci.*, 2016, **7**, 1088, DOI: 10.3389/fpls.2016.01088.